https://doi.org/10.5194/egusphere-2026-6684
Preprint. Discussion started: 16 November 2026
© Author(s) 2026. CC BY 4.0 License.

CO_2 carbonation and wave properties in mixtures of basalt and red mud

Mamdoh Alajmi[1], José M. Carcione[2,3], Ayman N. Qadrouh[1], Suhail S. Alhejji[4], and Jing Ba[2]

[1]KACST, PO Box 6086, Riyadh 11442, Saudi Arabia
[2]School of Earth Sciences and Engineering, Hohai University, Nanjing, China
[3]National Institute of Oceanography and Applied Geophysics – OGS, Trieste, Italy
[4]King Saud University, PO Box 2455, Riyadh 11451, Saudi Arabia

Correspondence: Jing Ba (jingba@188.com)

Abstract.

Red mud is a highly industrial by-product with potential for CO_2 mineralization, while basalt provides reactive minerals and further enhances carbonation. This work investigates the CO_2 carbonation of a mixture of basalt and red mud (in powder form). The study aims to propose a theoretical methodology to evaluate the weight of CO_2 in the mixture as a function of reaction time. In addition, we propose a model to obtain the P- and S-wave velocities before and after carbonation of the mixture, which is partially saturated with water. The model considers the mineral composition of the basalt and red mud grains, compaction, temperature, water saturation, and grain size. Velocities and mass density increase with compaction, while porosity decreases. Carbonation and velocities are enhanced by higher temperature and smaller grain sizes, while compaction slightly decreases CO_2 absorption.

1 Introduction

A viable strategy for lowering the quantity of greenhouse gasses in the atmosphere is to store carbon dioxide (CO_2) in basalt and red mud, which are rich in reactive and divalent cations. The Jizan Group, a rich sequence of Oligocene basalts that formed along the continental rift before to the entrance of the Red Sea, is located along Saudi Arabia's southwest coast (Oelkers et al., 2022). These basalts are intended for the disposal of CO_2 emitted from industrial sources through carbon mineralization in subsoil processes. Red mud (bauxite residue) is also a candidate for CO_2 storage. In Saudi Arabia, red mud is primarily produced at the large Ma'aden and Alcoa joint-venture aluminum complex in Ras Al Khair. According to the Ma'aden Annual Report in 2016, the Saudi Arabian Mining Company estimates bauxite ore reserves in Saudi Arabia at approximately 230 million tons (Alkhammali et al., 2018; Almutairi et al., 2026).

Before CO_2 intake, uncarbonated red mud typically exists as a fine, slurry-like or uncompacted granular material with high initial porosity. Because of its high alkalinity and the presence of free sodium and calcium hydroxides, fresh red mud generally has low acoustic wave velocity, which depends strongly on water saturation. Exposing basalt and red mud to CO_2 changes their elastic properties through mineral carbonation. This process converts alkaline hydroxides into carbonates such as calcite

https://doi.org/10.5194/egusphere-2026-6684
Preprint. Discussion started: 16 November 2026
© Author(s) 2026. CC BY 4.0 License.

($CaCO_3$), reducing porosity, increasing matrix density, and ultimately raising ultrasonic velocity and elastic moduli by grain cementation.

Yadav et al. (2010) found that calcium bearing mineral phases, chantalite and cancrinite, are the mineral phases responsible for the carbonation of red mud, with a carbonation capacity of 53 g of CO_2 per kg of red mud at 3.5 h reaction time. They considered reaction times of 0.5–12 h at an average pressure of 3.5 bar (0.35 MPa). The main chemical components of red mud are SiO_2, Al_2O_3, Fe_2O_3, CaO and Na_2O, depending on the bauxite source and production process (see Fig. 5 in Liu et al., 2024). The carbon uptake of red mud is 5–175 g of CO_2 per kg of red mud, depending on the composition and carbonation pathway. CO_2 uptake increases with pore pressure, temperature and reaction times (e.g., Fig. 10 in Liu et al., 2024).

Mucsi et al. (2021) studied CO_2 sequestration behavior in red mud at 25 °C and 5 bar (0.5 MPa) and found that mechanical activation enhances the ability of red mud to uptake CO_2. Soluble Na-carbonates provide less permanent CO_2 storage than solid Ca-Mg-carbonates because of their solubility. Alkaline earth metal ions, such as calcium or magnesium, enhance carbonation, which depends on water saturation. If it is low the reactions halt because there is not enough moisture to dissolve the ions. For full saturation, water blocks the pore network, preventing CO_2 from diffusing inward. Intermediate water saturation allows for the perfect balance of CO_2 gas diffusion and ion dissolution. Zeng et al. (2025) investigated CO_2 sequestration in red mud solution from 20 to 80 °C for reaction times of up to 70 min. The main component is CaO. The carbonation first increased and then decreased with rising temperature, reaching an optimal carbonation effect at 60 °C, where approximately 80 g of CO_2 was sequestered per kg of red mud.

Experiments in basalt are reported by Adam et al. (2013). Carcione et al. (2023) considered carbonation of basalt and computed the post-carbonation wave velocities using a cementation model. Here, we consider an alternative rock-physics model applied to a mixture of basalt and red mud. Similar to a diagenesis process, the mineralization process reduces porosity when minerals precipitate from solution and cement grain contacts and fill fissures (e.g., Carcione et al., 2023). There has not been any theoretical discussion of the acoustics of mineralization and cementation. The mineralization approach starts by a computation of the volume of carbonate cement precipitated by using a modified Walderhaug (1996) model, which gives the fraction of cements and porosity as a function of the reaction time. The process is dependent on the granules' surface area and effective radii; smaller grains yield more cement. The volume of precipitated carbonates is roughly equivalent to the porosity loss. The rock's wave velocities are obtained using a petro-elastic model. The approach is based on the Hashin-Shtrikman equation to compute the properties of the grains and the Hertz-Mindlin-Athy-Gassmann model to obtain the pre- and post-carbonation elastic velocities of the partially saturated medium.

To our knowledge, there are no models relating the effects of carbon mineralization in red mud on elastic velocities. Existing red-mud CO_2 sequestration studies are mostly experimental. Basically, the paper is substantially theoretical and the objectives are (i) to develop a time-dependent model for calculating CO_2 uptake mass in basalt-red-mud powder mixtures; (ii) to build a petro-elastic model predicting P- and S-wave velocities before and after partial-water-saturation carbonation; and (iii) to quantify the sensitivity of CO_2 sequestration and acoustic properties to compaction, temperature, grain size, and water saturation.

https://doi.org/10.5194/egusphere-2026-6684
Preprint. Discussion started: 16 November 2026
© Author(s) 2026. CC BY 4.0 License.

2 Pre-carbonation elastic properties of the basalt–red mud mixture

In a typical laboratory experiment, basalt and red mud powder are mechanically dry-blended until a homogeneous mixture is achieved. Controlled water content (12–15 wt% of the total dry mixture) is then added and the mixture is remixed until uniform moisture is obtained. The mixture is compacted using a hydraulic press under ambient conditions. The powder is expected to enhance reaction efficiency due to its higher surface area. To compute the elastic properties, it is necessary to evaluate the effective bulk (K) and shear (μ) moduli of the solids.

In basalt, we consider the chemical compositions given in Table 1 of Kanakiya et al., 2017, core ID: P5), but reduce the components to five: In weight percent: 15 % of Fe_2O_3, 15 % of Al_2O_3, 45 % of SiO_2, 13 % of MgO, and 12 % of CaO. The chemical compositions of Bayer red mud is 13.69 % of Fe_2O_3, 7.02 % of Al_2O_3, 18.1 % of SiO_2, 2.38 % of Na_2O, 42.21 % of CaO, 2.1 % of TiO_2 and 0.3 % of K_2O (Wang et al. 2019), further simplified to 20 % of Fe_2O_3, 6 % of Al_2O_3, 15 % of SiO_2, 9 % of Na_2O, 50 % of CaO. We have considered the main components, since small percentages have a minor effect. However, the theory is general and does not preclude using more components.

If the amount of basalt in the mixture is β, the weight percent of each element in the mixture is

$$\beta \cdot (\text{weight \% in basalt}) + (1-\beta) \cdot (\text{weight \% in red mud}). \tag{1}$$

Here we assume $\beta = 0.5$, i.e. equal composition. Table 1 gives the bulk and shear moduli and density of each component. (e.g., Mavko et al., 2020). The volume percent of a given component is calculated as

$$\text{volume } (\%) = 100 \cdot \frac{\text{weight } (\%)}{\text{density} \cdot \text{total volume}}, \tag{2}$$

where total volume is the sum of the partial volumes, each calculated as the weight in grams divided by the density of each component. Based on the above proportions (those of Table 1 correspond to the mixture basalt-red mud), for basalt (index 1) and red mud (index 2), a Hashin-Shtrikman average (see Appendix A) gives K_1 = 63.3 GPa, μ_1 = 62.8 GPa, and K_2 = 80.7 GPa, μ_2 = 65 GPa, for the mineral grains. The composite mineral densities are arithmetic averages and we obtain ρ_1 = 3245 kg/m^3 and ρ_2 = 3348 kg/m^3, respectively.

To obtain the wave velocities and density of the mixture as a function of the confining pressure, we use the Hertz-Mindlin-Athy-Gassmann (HMAG) model given in Appendix B. As stated above, we assume a proportion of basalt of β = 50%. The composite mineral bulk and shear moduli are K = 71.5 GPa and μ = 63.9 GPa, according to equations (B1). The average number of contacts per grain is C = 6.2, ϕ_0 = 0.36, p_b = 0.1 MPa and p_r = 3 MPa. The water bulk modulus and density are K_f = 2.25 GPa and ρ_w = 1000 kg/m^3, respectively, and the water saturation is S_w = 1. Figure 1 shows the wave velocities (a), and porosity and density (b) as functions of confining pressure. As expected, with compaction, the velocities increase with pressure, the porosity decreases, and the density increases. The porosity at 1 MPa is 26%.

https://doi.org/10.5194/egusphere-2026-6684
Preprint. Discussion started: 16 November 2026
© Author(s) 2026. CC BY 4.0 License.

3 CO_2 Carbonation

The total weight percent of the basalt-red mud mixture is reported in Table 1, along with the elastic moduli, density, volume percent, and molar mass of the components (e.g., Mavko et al., 2020). The volume percent of a given component is calculated by using equation (2). We consider stable carbonates under ambient conditions and exclude aluminium and silicon. Compaction corresponds to the confining pressure of 1 MPa, with a porosity of 26% (see Figure 1b). Roughly, these components react with a CO_2-water mixture, resulting in the precipitation of minerals (Fe, Na, Mg and Ca cations) at grain contacts (cementation). The first reaction is the formation of carbonic acid:

$CO_2 + H_2O \rightarrow H_2CO_3$ (carbonic acid)

Then, those cations precipitate as carbonates as:

(Fe, Na, Mg, Ca) + $H_2CO_3 \rightarrow$ (Fe, NaH, Mg, Ca) CO_3.

The carbonation model is given in Appendix C. In this case, we consider a water saturation S_w = 0.2. We set the grain diameter of the basalt and red-mud grains equal to D = 75 μm. Moreover, we consider the following properties: ϕ (1 MPa) = 0.26, $a = 2.2 \times 10^{-3}$ mol/m^5, and

$$b = (10 + 0.4T) \times 10^{-7}, \tag{3}$$

in 1/s, with T given in °C (see equation (C6)). This equation holds till approximately 60 °C. During the initial stage of carbonation, the conversion rate increases with temperature. However, beyond a certain temperature threshold ($\approx$ 60 °C), higher temperatures result in lower carbonation degrees (e.g., Rushendra Revathy et al. 2021; Zeng et al., 2025)

We consider T = 20 °C, and the time step to solve equation (C1) is dt = 0.12 h. Figure 2 shows the cement fraction for the four carbonates as a function of time (a) and the total porosity (b). The first row in Table 2 presents the volume fractions of the stable carbonates calculated using the equations in Appendix C. Densities and weight fractions are also provided.

Let us denote the cation by X_k, k = 1, 4. To obtain the mass of CO_2 uptake in 1 kg of carbonated basalt-red mud mixture at 72 h, we first compute the mass of XCO_3 in 1 m^3:

$$m_{X_k} = \phi_p \rho_{X_k}, \tag{4}$$

where ρ_{X_k} is the density of the component, given in Table 2. The CO_2 mass fraction in XCO_3 is

$$w_k = \frac{\text{molar mass of } CO_2}{\text{molar mass of } XCO_3}, \tag{5}$$

such that the total mass of CO_2 in V = 1 m^3 is

$$m_V = \sum_k m_{X_k} w_k. \tag{6}$$

Now, we need to convert mass per volume to mass per total mass of basalt-red mud mixture. The average density of the basalt-red mud mixture is approximately the initial one.

$$\rho_b = \phi S_w \rho_w + (1 - \phi) \sum \phi_k \rho_k, \tag{7}$$

https://doi.org/10.5194/egusphere-2026-6684
Preprint. Discussion started: 16 November 2026
© Author(s) 2026. CC BY 4.0 License.

where ϕ is the initial porosity, S_w is the water saturation, ρ_w is the water density, and ϕ_k and ρ_k are the volume fraction and density of the components given in Table 1. We could have considered the bulk density at time t. In this case, the porosity of the medium is given by

$$\phi \to \phi - \sum_k \phi_p, \tag{8}$$

and the second term on the right-hand side of equation (7) becomes

$$(1-\phi)\left\{\sum_k [(\phi_k - \phi_p(k)]\rho_k + \phi_p(k)\rho'_k\right\},$$

where ρ'_k is the density of the carbonates given in Table 2. However, the result is approximately the same. We assumed that the contribution of air and CO_2 is negligible, since water is more than 500 times as dense than these elements at ambient conditions.

Then, the amount of CO_2 uptake in grams in W = 1 kg is

$$m_W[\mathrm{g}] = 1000[g] \cdot \frac{m_V}{\rho_b} \tag{9}$$

where m_V is given in kg of CO_2 per m^3 and ρ_b in kg of mixture per m^3.

Table 2 lists the partial values (4th and 5th rows), corresponding to each carbonate. The total values are m_V = 58.81 kg/m^3 and m_W = 23.61 g/kg. Typical values in red mud are 5–175 g of CO_2 per kg (e.g., Liu et al., 2024).

On the other hand, to obtain the amount of CO_2 uptake in grams in $W = 1$ kg as a function of the reaction time t for each component, we first obtain

$$m_{Vk}(t) = m_{\mathrm{X}k}(t) w_k. \tag{10}$$

The composite density is taken the initial one (7). Then

$$m_{Wk}(t)[\mathrm{g}] = 1000[g] \cdot \frac{m_{Vk}}{\rho_b}. \tag{11}$$

The sum on k gives the total mass of CO_2 per kg of mixture:

$$m_W(t)[\mathrm{g}] = \sum_k m_{Wk}(t). \tag{12}$$

Figure 3 shows m_W as a function of reaction time at two temperatures and 1 MPa compaction.

The compaction pressure mainly affects the initial porosity. We have seen that at 1 MPa, ϕ = 0.26 pre-carbonation, while at 0.3 and 0.1 MPa, $\phi \approx$ 0.33 and 0.36, respectively (see Figure 1b). Confining pressure (compaction) exerts only a weak effect on carbonation unless it pushes CO_2 into a supercritical state, which is not the case here, since pore pressures are below 7 MPa. The CO_2 carbonation (or mineralization) rate decreases with increasing confining pressure under ambient conditions. Higher confining pressure compacts the material, reducing interconnected pore space. This restricts CO_2 gas diffusion into the matrix,

https://doi.org/10.5194/egusphere-2026-6684
Preprint. Discussion started: 16 November 2026
© Author(s) 2026. CC BY 4.0 License.

slowing the chemical reaction. This behavior can be observed in Figure 3, where we plot m_W as a function of reaction time for three pressures at T = 20 °C.

Next, we consider a grain diameter D = 50 μm and compare the results to the case D = 75 μm at 20 °C and a compaction pressure of 1 MPa. It has been observed experimentally (Mucsi et al., 2021) that grinding or mechanically activating the material reduces particle size and increases surface area, exposing more reactive alkaline minerals (such as calcium and sodium) to CO_2 and enhancing the reaction. Figure 5 shows the results.

4 Post-carbonation elastic properties of the basalt–red mud mixture

We consider that the medium reacts with CO_2 and obtain the elastic properties using the HMAG model given in Appendix C. In Carcione et al. (2023), we considered a petro-elastic model for basaltic rock based on the contact-cement theory of Dvorkin and Nur (1996), which assumes cement is deposited at grain contacts, and the Hertz-Mindlin (HM) theory. The Voigt-Reuss-Hill averages and the Gassmann equation provide the wet-rock moduli, while the self-consistent (SC) model is used to obtain the properties of the mineral mixture. Here, the cementation model is simpler, based on a modification of the Hertz-Mindlin model with a single parameter, the cementation exponent, since we have a compacted powder composed of particles. An alternative more complex model is Dvorkin and Nur's contact-cement theory, as used in Carcione et al. (2023), which can be applied as an extension of this work.

Compared to pre-carbonation, the bulk density and grain properties change due to the generation of carbonates. As indicated above, the bulk density (7) becomes

$$\rho_b = \phi S_w \rho_w + (1-\phi)\left\{\sum_k [(\phi_k - \phi_p(k)]\rho_k + \phi_p(k)\rho_k'\right\}, \tag{13}$$

where ϕ is given by equation (8) and ρ_k' is the density of the carbonates given in Table 2.

First, we need to compute the composite or effective mineral elastic moduli and density. The mineral is composed of the initial elements (Table 1) and carbonates (Table 2). At reaction time t, the initial elements have proportions $\phi_k - \phi_p(k)$, and the carbonates have proportion $\phi_p(k)$, such that the sum is $\sum_k \phi_k = 1$. We apply the Hashin-Shtrikman average, assuming the proportion of reacted Al and Si is zero (no carbonation for these elements). We have six initial minerals with moduli given in Table 1 and four carbonates with elastic moduli given in Table 2. In this case, we apply the Hashin-Shtrikman average, which gives K = 71 GPa and μ = 63.5 GPa at t = 0, and K = 69.8 GPa and μ = 61.5 GPa at 72 h, instead of the Voigt-Reuss average (B1), which gives K = 71.5 GPa and μ = 63.9 GPa. The result is shown in Figure 6. Since carbonates are softer, velocities and density decrease with reaction time.

Cementation mainly affects the degree of bonding p_b of the grains in equation (B5), and therefore the dry-rock elastic moduli K_m and μ_m. Gangi (1978) interprets $p_b = P_i$ as the equivalent pressure due to the cementation. We assume that

$$p_b = p_a\left\{1 + m\sum_k \phi_p(k)(\%)\right\} \tag{14}$$

https://doi.org/10.5194/egusphere-2026-6684
Preprint. Discussion started: 16 November 2026
© Author(s) 2026. CC BY 4.0 License.

where ϕ_p is given in Table 2, p_a is the atmospheric pressure (0.1 MPa), and $m > 1$ is an empirical parameter determined experimentally. Figure 7 shows p_b as a function of reaction time, and Figure 8 shows the corresponding wave velocities (a) and density (b). The compaction pressure is 0.2 MPa, and $m = 10$ in equation (14). As expected, velocity increases with reaction time due to the cementation of the grains.

To further verify the consistency of the model, we show in Figure 9 the post-carbonation P-wave velocities as a function of reaction time for two grain sizes. As can be seen, velocity increases with decreasing grain radius, since more surface area enhances the carbonation.

5 Conclusions

We present a quantitative model to simulate the CO_2 carbonation of a basalt and red mud mixture under ambient conditions, obtaining P- and S-wave velocities as functions of reaction time, compaction, temperature, water saturation, grain diameter, and mineralization of the matrix as carbonate cements. The velocities are calculated using the Hashin-Shtrikman and Hertz-Mindlin-Athy-Gassmann models. Mineralization is based on a model that estimates the volume of precipitated carbonates and the resulting porosity loss, and post-carbonation velocities as a function of reaction time are calculated with the same petrophysical model by including an equivalent pressure parameter due to cementation. Velocities and mass density increase with compaction, while porosity decreases. Carbonation and velocities are enhanced by higher temperature and smaller grain diameters, while compaction slightly decreases CO_2 absorption. Extensions of the present model involve different proportions of basalt and red mud, the effect of pore pressure (e.g., supercritical CO_2), and the description of wave attenuation.

Moreover, we are initiating laboratory experiments in KACST using the same basalt–red mud mixtures considered in the model. The powders will be dry mixed, followed by the addition of a controlled amount of water as a binding medium prior to compaction. These experiments will provide essential data to validate and refine the numerical model, strengthening the connection between the modeling framework and its experimental verification. However, the developed model is intended not only for laboratory sample interpretation, but also for field geophysical monitoring of in-situ mineral carbonation.

https://doi.org/10.5194/egusphere-2026-6684
Preprint. Discussion started: 16 November 2026
© Author(s) 2026. CC BY 4.0 License.

Appendix A: Grain stiffness moduli

Defining the solid proportions by p_i, for n minerals, the following relation holds

$$\sum_{i=1}^{n} p_i = 1. \tag{A1}$$

The Hashin-Shtrikman upper $(+)$ and lower $(-)$ bounds for the bulk and shear moduli are

$$\begin{aligned} K^{\mathrm{HS}\pm} &= \Lambda(\mu_\pm), \\ \mu^{\mathrm{HS}\pm} &= \Gamma[\xi(K_\pm, \mu_\pm)], \end{aligned} \tag{A2}$$

where

$$\Lambda(\mu_\pm) = \left\langle \frac{1}{K + \frac{4}{3}\mu_\pm} \right\rangle^{-1} - \frac{4}{3}\mu_\pm, \tag{A3}$$

$$\Gamma(\xi) = \left\langle \frac{1}{\mu + \xi} \right\rangle^{-1} - \xi, \tag{A4}$$

$$\xi(K_\pm, \mu_\pm) = \frac{\mu_\pm}{6}\left(\frac{9K_\pm + 8\mu_\pm}{K_\pm + 2\mu_\pm}\right) \tag{A5}$$

(e.g., Mavko et al., 2020), and the subscripts $+$ and $-$ denote the maximum and minimum moduli of the single constituents. The brackets $\langle \cdot \rangle$ indicate an average over the constituents weighted by their volume fractions. The density is simply the arithmetic average of the densities of the single constituents weighted by the corresponding volume fractions.

The arithmetic averages of the bounds are frequently used to obtain the bulk and shear moduli of a mineral mixture, i.e.,

$$K_s = \frac{1}{2}(K^+_{\mathrm{HS}} + K^-_{\mathrm{HS}}), \quad \mu_s = \frac{1}{2}(\mu^+_{\mathrm{HS}} + \mu^-_{\mathrm{HS}}). \tag{A6}$$

Appendix B: The Hertz-Mindlin-Athy-Gassmann (HMAG) model

The effective elastic properties of the grains of a mixture of basalt and red-mud can be obtained with the Voigt-Reuss-Hill average, i.e., an arithmetic average of the Voigt and Reuss moduli (e.g., Mavko et al., 2020). Let K_1 and μ_1 be the bulk and shear moduli of the basalt particles, and K_2 and μ_2 those of the red-mud particles. The effective moduli are

$$K = \frac{1}{2}(K_V + K_R) \quad \text{and} \quad \mu = \frac{1}{2}(\mu_V + \mu_R), \tag{B1}$$

https://doi.org/10.5194/egusphere-2026-6684
Preprint. Discussion started: 16 November 2026
© Author(s) 2026. CC BY 4.0 License.

where

$$K_V = \beta K_1 + (1-\beta)K_2, \quad \text{and} \quad \mu_V = \beta\mu_1 + (1-\beta)\mu_2, \tag{B2}$$

and

$$\frac{1}{K_R} = \frac{\beta}{K_1} + \frac{1-\beta}{K_2}, \quad \text{and} \quad \frac{1}{\mu_R} = \frac{\beta}{\mu_1} + \frac{1-\beta}{\mu_2}, \tag{B3}$$

where β is the fraction of basalt. The effective density is simply

$$\rho_s = \beta\rho_1 + (1-\beta)\rho_2, \tag{B4}$$

where ρ_1 and ρ_2 are the basalt and red-mud particle densities, respectively.

The elastic properties of a compacted powder saturated with a fluid can be determined by combining the Hertz-Mindlin (HM) model with the Gassmann equation. The Hertz-Mindlin contact theory considers a random packing of spheres as an effective medium (Mavko et al., 2020, Eqs 5.5.37 and 5.5.41; Carcione et al., 2023). The bulk and shear dry-rock moduli are

$$K_m = \left[\frac{C^2[1-\phi(p_c)]^2\mu^2(p_c+p_b)}{18\pi^2(1-\nu)^2}\right]^{1/3} \tag{B5}$$

and

$$\mu_m = \frac{3(5-4\nu)}{5(2-\nu)}K_m, \tag{B6}$$

where p_c is the confining pressure, and p_b is the degree of bonding by cementation (Gangi (1978) interprets $p_b = P_i$ as the equivalent pressure due to the cementation). Initially, p_b is a pre-stress pressure, assumed to be the atmospheric pressure pre-carbonation: 0.1 MPa). Moreover, ϕ is the porosity,

$$\nu = \frac{3K-2\mu}{2(3K+\mu)} \tag{B7}$$

is the Poisson ratio of the grains, and C is the average number of contacts per spherical grain. Porosity slightly decreases with pressure and can be expressed as

$$\phi = \phi_0 \exp(-p_c/p_r), \tag{B8}$$

(Athy, 1930; Kunin and Yurchenko, 1967), where we assume ϕ_0 = 0.36, and p_r= 3 MPa (see Carnavas and Page, 1998, for alternative models).

The wet-rock moduli are obtained with the Gassmann equations (e.g., Mavko et al., 2020; Carcione, 2022). The bulk and shear moduli are given by

$$K_G = K_m + \alpha^2\mathcal{M}, \quad \mu_G = \mu_m, \tag{B9}$$

where

$$\mathcal{M} = \left(\frac{\alpha-\phi}{K} + \frac{\phi}{K_f}\right)^{-1}, \tag{B10}$$

https://doi.org/10.5194/egusphere-2026-6684
Preprint. Discussion started: 16 November 2026
© Author(s) 2026. CC BY 4.0 License.

$$\alpha = 1 - \frac{K_m}{K}. \tag{B11}$$

and K_f is the fluid modulus.

The P-wave modulus and velocity are

$$E = K_G + \frac{4}{3}\mu_G. \tag{B12}$$

and

$$V_P = \sqrt{\frac{E}{\rho}}, \tag{B13}$$

respectively, where ρ is the composite density, given by

$$\rho = (1-\phi)\rho_s + \phi\rho_f, \tag{B14}$$

where ρ_s and ρ_f are the densities of the solid phase and fluid, respectively. If ρ_w, ρ_a and ρ_g are the water, air and CO_2 densities, the fluid density is

$$\rho_f = S_w\rho_w + S_g\rho_g + (1 - S_w - S_g)\rho_a, \tag{B15}$$

where S_w and S_g are the water and CO_2 saturations.

Similarly, the S-wave velocity is

$$V_S = \sqrt{\frac{\mu_G}{\rho}}. \tag{B16}$$

Appendix C: Walderhaug model of carbonation

We use the mathematical form of the Walderhaug (1996) model for the carbonation of minerals in basalt and red mud, which act as cement at grain contacts. The amount of cement (m^3) of a given component carbonated in 1 m^3 at time t_{l+1} is

$$\phi_p^{l+1} = \phi_i - (\phi_i - \phi_p^l)\exp\left[-\frac{aMA_0}{\rho_1\phi_i}\left(10^{bt_{l+1}} - 10^{bt_l}\right)\right], \tag{C1}$$

where ϕ_p^l is the amount of mineral cement present at time t_l, ϕ_i is the initial porosity, a and b are constants, which have units of mol/m^5 and s^{-1}, respectively, ρ_1 is the grain density, M [kg/mol] is the molar mass of mineral, and

$$A_0 = \frac{6V}{D} \tag{C2}$$

is the initial mineral specific surface area in m^2, where D is the grain diameter, and V is a unit volume (1 m^3 if D is given in meters)[1].

[1]We use a modified version of the Walderhaug (1996) model. In his Eqs. 3 and 8, b has units of inverse temperature, where the exponent is $b(ct+d) = bct + bd$. Here, $bc \to b$ and $a10^{bd} \to a$, and the new b depends on temperature.

https://doi.org/10.5194/egusphere-2026-6684
Preprint. Discussion started: 16 November 2026
© Author(s) 2026. CC BY 4.0 License.

In the first time step, $t_0 = 0$, $\phi_p^0 = 0$, and

$$\frac{\phi_p^1}{\phi_i} = 1 - \exp\left[-\frac{aMA_0}{\rho_1 \phi_i}(10^{bt_1} - 1)\right], \quad t_1 = dt, \tag{C3}$$

where dt is the time step.

The porosity varies as

$$\phi = \phi_i - \phi_p \quad (\phi^l = \phi_i - \phi_p^l) \tag{C4}$$

and the surface area as

$$A = A_0 \frac{\phi}{\phi_i}. \tag{C5}$$

We introduce temperature into parameter b as

$$b = \alpha T + \gamma, \tag{C6}$$

where α and γ are constants determined experimentally.

https://doi.org/10.5194/egusphere-2026-6684
Preprint. Discussion started: 16 November 2026
© Author(s) 2026. CC BY 4.0 License.

Code availability: The code underlying this article will be shared on reasonable request to the corresponding author.

Data availability: No new data were generated or analysed in support of this research.

Author contribution: Mamdoh Alajmi: conceptualization, methodology, software, formal analysis, writing – original draft. José M. Carcione: conceptualization, methodology, formal analysis, validation, writing – review and editing. Ayman N. Qadrouh: investigation, validation, writing – review and editing. Suhail S. Alhejji: investigation, resources, writing – review and editing. Jing Ba: conceptualization, methodology, formal analysis, supervision, writing – review and editing.

Competing interests: The authors declare that they have no conflict of interest.

https://doi.org/10.5194/egusphere-2026-6684
Preprint. Discussion started: 16 November 2026
© Author(s) 2026. CC BY 4.0 License.

References

Adam, L., Wijk, K., Otheim, T., and Batzle, M., 2013, Changes in elastic wave velocity and rock microstructure due to basalt-CO2-water reactions, J. Geophys. Res. Solid Earth, 118, 4039–4047, https://doi.org/10.1002/jgrb.50302

Alkhammali, S. A. et al., 2018, Mineralogical and geochemical analyses of red mud in Saudi Arabia, 2nd Conference of Bauxite Residue Valorisation and Best Practices, Athens, Greece. https://conference2018.redmud.org/programme-br2018/

Almutairi, A. N. et al., 2026, Economic insights from the Al Ba'itha Mine, Saudi Arabia, Minerals, 2026, 16(10), 1050; https://www.mdpi.com/2075-163X/16/10/1050

Athy L. F., 1930, Density, porosity and compactation of sedimentary rocks, Bull. Amer. Assoc. Petrol. Geol., 14, 1–2. https://pubs.geoscienceworld.org/aapg/aapgbull/article-abstract/14/1/1/544454/Density-Porosity-and-Compaction-of-Sedimentary?redirectedFrom=fulltext

Carcione, J. M., 2022, Wave Fields in Real Media. Theory and numerical simulation of wave propagation in anisotropic, anelastic, porous and electromagnetic media, 4th edition, revised and extended, Elsevier Science. https://doi.org/10.1016/C2021-0-00938-X

Carcione, J. M., Qadrouh, A. N., Alajmi, M., Alqahtani, N. B., and Ba, J., 2023, Rock acoustics of CO_2 storage in basalt, Geophys, J. Internat., 234(3), 2429–2435. https://doi.org/10.1093/gji/ggad252

Carnavas, P. C., and Page, N. W., 1998, Elastic properties of compacted metal powders. J. Mat. Science, 33, 4647–4655. https://doi.org/10.1023/A:1004445527430

Dvorkin , J., and Nur, A., 1996, Elasticity of high-porosity sandstones: theory for two North Sea data sets, Geophysics, 61, 1363–1370. https://doi.org/10.1190/1.1444059

Gangi A.F., 1978, Variation of whole and fractured porous rock permeability with confining pressure, International Journal of Rock Mechanics and Mining Sciences 15, 249–257. https://doi.org/10.1016/0148-9062(78)90957-9

Kanakiya , S. , Adam, L., Esteban, L., Rowe, M. C., and Shane, P., 2017. Dissolution and secondary mineral precipitation in basalts due to reactions with carbonic acid, J. Geophys. Res., 122, 4312–4327. https://doi.org/10.1002/2017JB014019

Kunin, N. F., and Yurchenko, B. D., 1967, Porosity versus pressure during the compacting of powders and probabilistic nature of densification law. Powder Metall. Met. Ceram., 6, 953–957. https://doi.org/10.1007/BF00779956

Liu, X., Liu, X., and Zhang, Z., 2024, Application of red mud in carbon capture, utilization and storage (CCUS) technology, Renewable and Sustainable Energy Reviews, 202, 114683. https://doi.org/10.1016/j.rser.2024.114683

https://doi.org/10.5194/egusphere-2026-6684
Preprint. Discussion started: 16 November 2026
© Author(s) 2026. CC BY 4.0 License.



Mavko, G., Mukerji, T., and Dvorkin, J., 2020, The Rock Physics Handbook, third edition. Cambridge Univ. Press. https://doi.org/10.1017/9781108333016

Mucsi, G., Halyag, N., Kurusta, T., and Kristály, F., 2021, Control of carbon dioxide sequestration by mechanical activation of red mud, Waste and Biomass Valorization, 12, 6481–6495. https://doi.org/10.1007/s12649-021-01466-2

Oelkers , E. et al. , 2022, The subsurface carbonation potential of basaltic rocks from the Jizan region of Southwest Saudi Arabia, Int. J. Greenhouse Gas Contl., 120, doi:10.1016/j.ijggc.2022.103772. https://doi.org/10.1016/j.ijggc.2022.103772

Rushendra Revathy, T. D., Ramachandran, A., and Palanivelu, K., 2021, Sequestration of CO_2 by red mud with flue gas using response surface methodology, Carbon Management, 12(2), 139–151. https://doi.org/10.1080/17583004.2021.1893127

Yadav, V. S., Prasad, M., Khan, J., Amritphale, S. S., Singh, M., and Raju, C. B., 2010, Sequestration of carbon dioxide (CO_2) using red mud Journal of Hazardous Materials, 176, 1044–1050. https://doi.org/10.1016/j.jhazmat.2009.11.146

Walderhaug, O., 1996, Kinetic modelling of quartz cementation and porosity loss in deeply buried sandstone reservoirs, AAPG Bulletin, 80, 731–745. https://doi.org/10.1306/64ED88A4-1724-11D7-8645000102C1865D

Wang, L., Hu, G., Lyu, F., Yue, T., Tang, H., Han, H., Yang, Y., Liu, R., and Sun, W., 2019, Application of red mud in wastewater treatment, Minerals, 9, 281; https://doi.org/10.3390/min9050281

Zeng, H., Bi, J., Zhao, Y., and Shen, M., 2025, The influence of temperature on the process of carbon dioxide fixation in sintered red mud and the mechanism of mineral phase evolution. Journal of Environmental Chemical Engineering, 13(5), 114321. https://doi.org/10.1016/j.jece.2025.119607

https://doi.org/10.5194/egusphere-2026-6684
Preprint. Discussion started: 16 November 2026
© Author(s) 2026. CC BY 4.0 License.

Table 1. Components and properties of the basalt-red mud mixture.

Property	Fe_2O_3	Al_2O_3	SiO_2	Na_2O	MgO	CaO
K (GPa)	100	140	37	46	160	115
μ (GPa)	95	90	44	30	130	81
Weight %	17.5	10.5	30	4.5	6.5	31
Density (g/cm^3)	5.25	3.98	2.65	2.27	3.58	3.35
Volume %	10.98	8.69	37.31	6.53	5.98	30.50
Molar mass (g/mol)	159.7	101.96	60.08	61.98	40.3	56.08

Table 2. Carbonate fractions of the basalt-red mud mixture and properties$^{(*)}$.

Property	$FeCO_3$	$NaHCO_3$	$MgCO_3$	$CaCO_3$
$\phi_p(\%)$	1	1.29	0.95	1.22
Density (g/cm^3)	3.9	2.16	2.96	2.71
Molar mass (g/mol)	115.85	84.01	84.31	100.1
m_V (kg of CO_2 in 1 m^3)	14.92	14.59	14.73	14.55
m_W (g of CO_2 in 1 kg)	6	5.86	5.91	5.84
K (GPa)	117	30	110	98
μ (GPa)	40	20	55	35

$(*)$ Reaction time: 72 h.

https://doi.org/10.5194/egusphere-2026-6684
Preprint. Discussion started: 16 November 2026
© Author(s) 2026. CC BY 4.0 License.

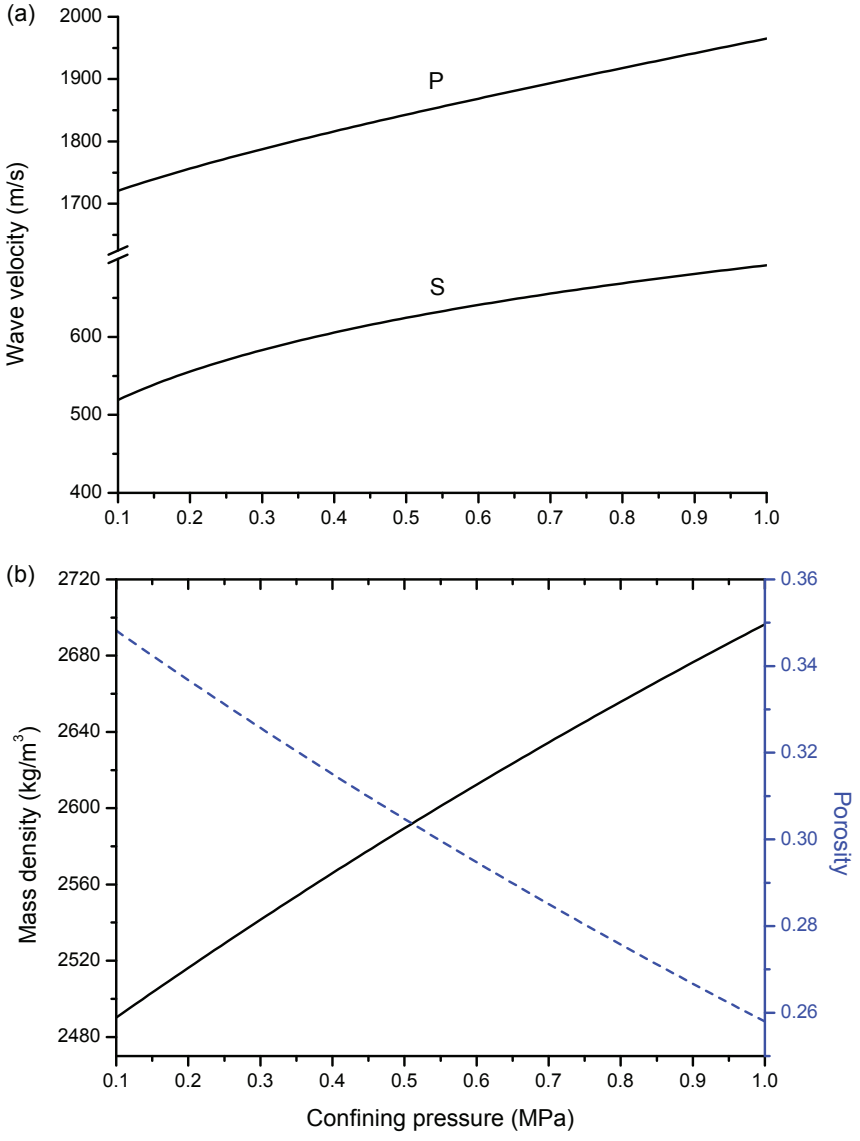


Figure 1. Pre-carbonation wave velocities (a), and density (solid line) and porosity (dashed line) (b) of a water saturated mixture of basalt and red mud as a function of confining pressure.Temperature is 20 °C and water saturation is 100 %

https://doi.org/10.5194/egusphere-2026-6684
Preprint. Discussion started: 16 November 2026
© Author(s) 2026. CC BY 4.0 License.

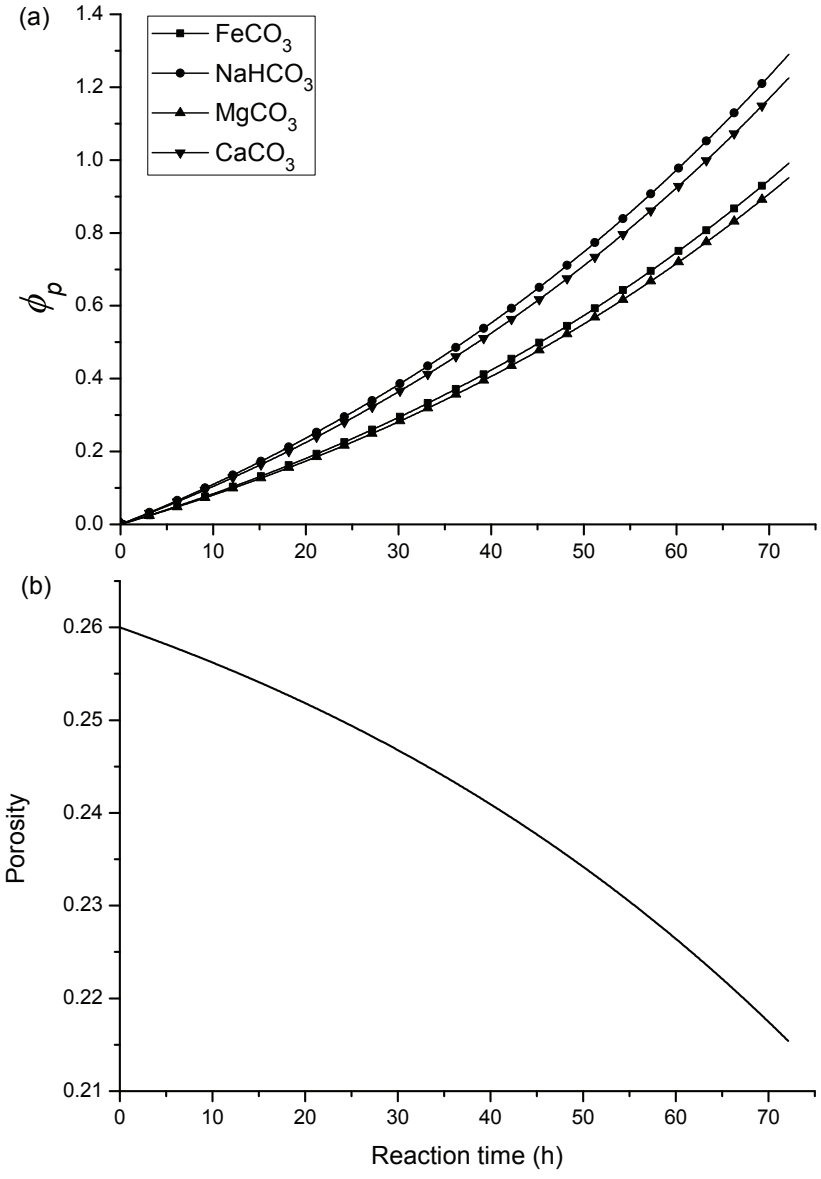


Figure 2. Volume fractions ϕ_p in % of each carbonate (a) and total porosity (b) as a function of reaction time. Temperature is 20 °C, and the basalt-red mud mixture is compacted at 1 MPa (phi = 26%, see Figure 1b), and water saturation is 20 %.

https://doi.org/10.5194/egusphere-2026-6684
Preprint. Discussion started: 16 November 2026
© Author(s) 2026. CC BY 4.0 License.

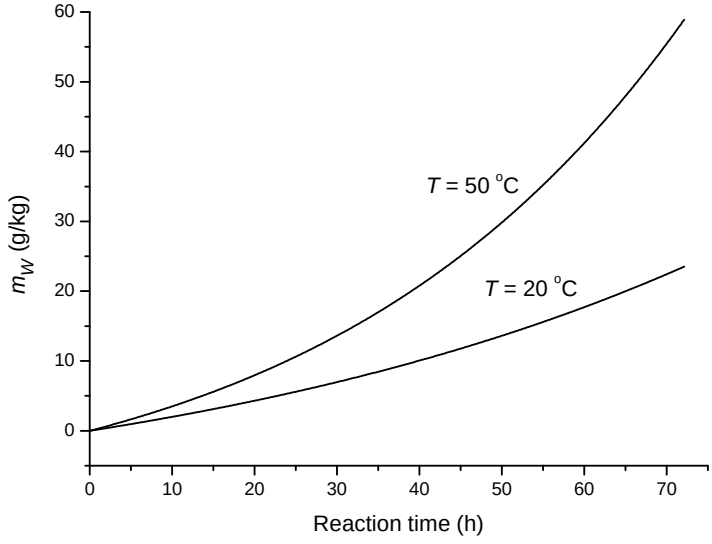


Figure 3. Total CO_2 mass as a function of reaction time (equation (12)) for two temperatures. The basalt-red mud mixture is compacted at 1 MPa (phi = 26%, see Figure 1b), and water saturation is 20 %.

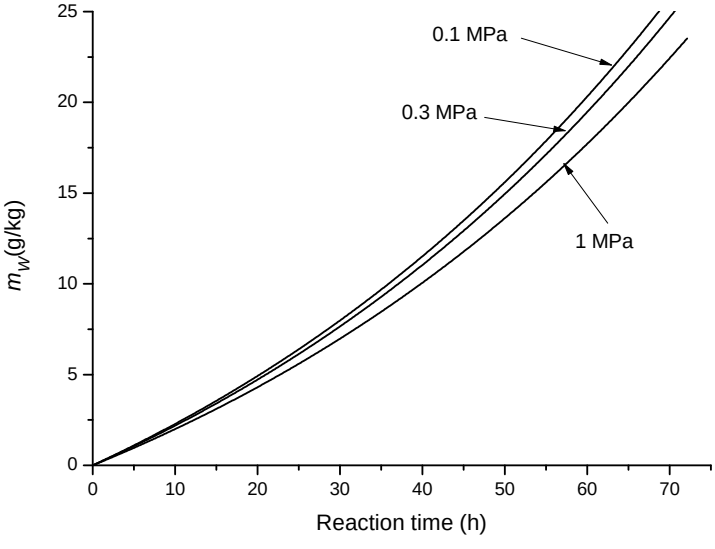


Figure 4. Total CO_2 mass as a function of reaction time (equation (12)) for three confining pressures (different compactions, see Figure 1b, for the porosities corresponding to the pressures indicated in the plot). Temperature is 20 °C, and water saturation is 20%.

https://doi.org/10.5194/egusphere-2026-6684
Preprint. Discussion started: 16 November 2026
© Author(s) 2026. CC BY 4.0 License.

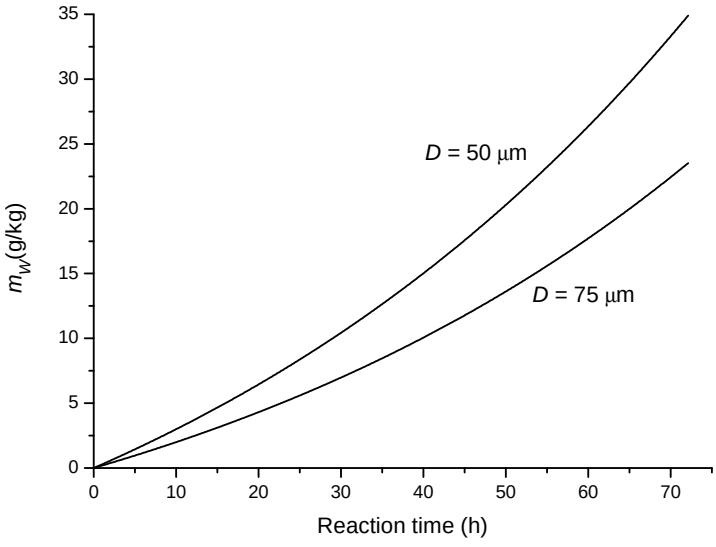


Figure 5. Total CO_2 mass as a function of reaction time (equation (12)) for two grain diameters. Temperature is 20 °C, compaction corresponds to 1 MPa (phi = 26%, see Figure 1b), and water saturation is 20%.

https://doi.org/10.5194/egusphere-2026-6684
Preprint. Discussion started: 16 November 2026
© Author(s) 2026. CC BY 4.0 License.

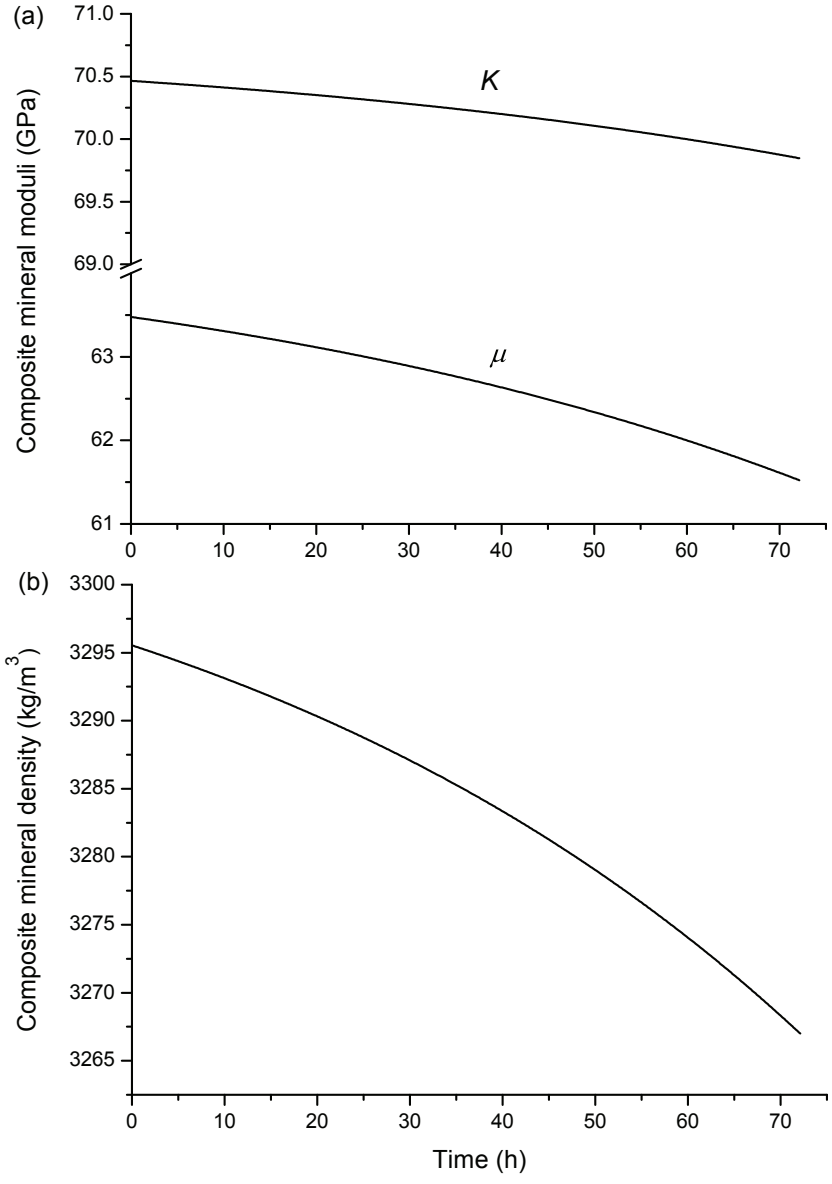


Figure 6. Composite mineral moduli (a) and density (b) post-carbonation as a function of reaction time.

https://doi.org/10.5194/egusphere-2026-6684
Preprint. Discussion started: 16 November 2026
© Author(s) 2026. CC BY 4.0 License.

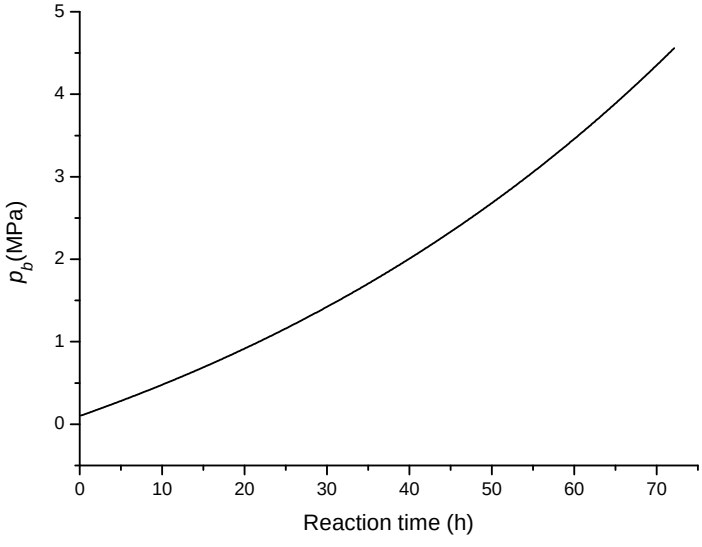


Figure 7. Cementation pressure as a function of reaction time.

https://doi.org/10.5194/egusphere-2026-6684
Preprint. Discussion started: 16 November 2026
© Author(s) 2026. CC BY 4.0 License.

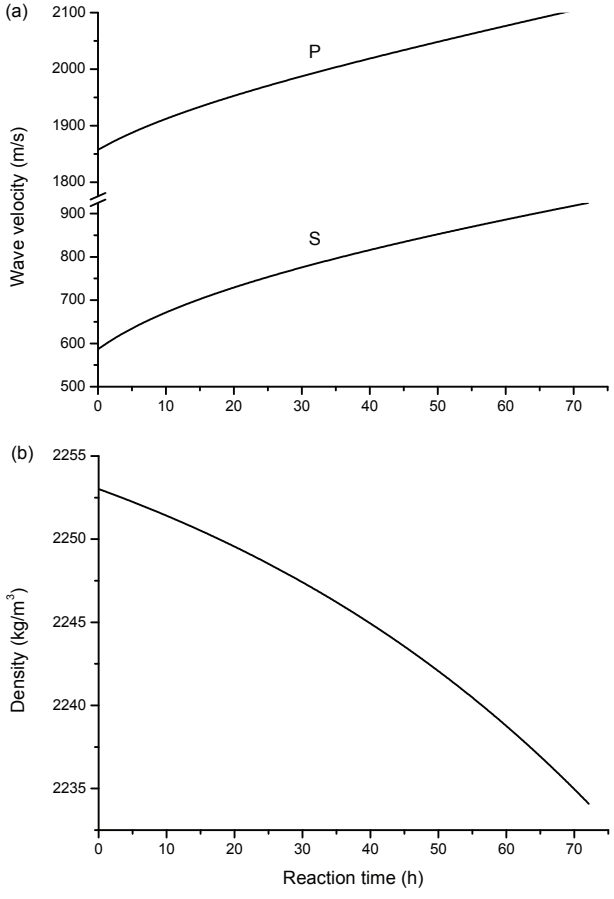


Figure 8. Post-carbonation wave velocities (a), and density (b) as a function of reaction time. The compaction pressure is p_c = 0.2 MPa and m = 10 in equation (14). Other parameters are T = 20 °C, D = 75 μm, C = 6.2, and ϕ_0 = 0.36.

https://doi.org/10.5194/egusphere-2026-6684
Preprint. Discussion started: 16 November 2026
© Author(s) 2026. CC BY 4.0 License.

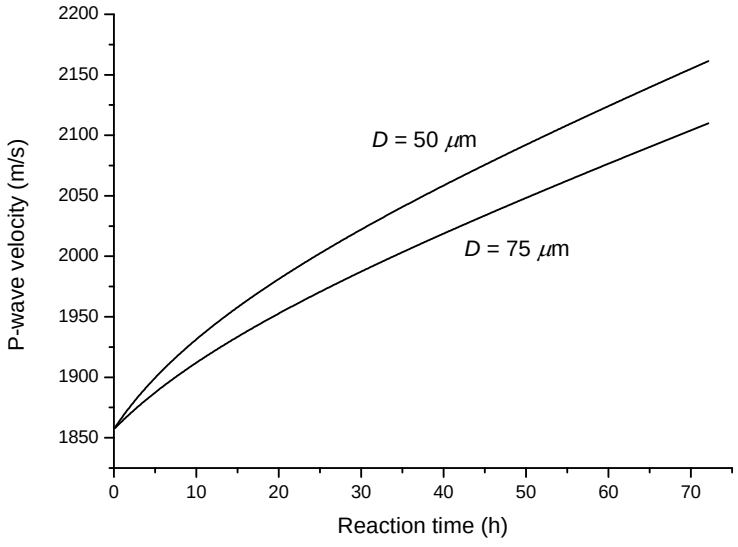


Figure 9. Post-carbonation P-wave velocities as a function of reaction time and two grain sizes. The conditions are the same as those in Figure 8.